SPECTRAL UNMIXING OF ROCK/MINERAL TARGETS BASED ON DIFFERENT SPATIAL RESOLUTION HYPERSPECTRAL DATA

Karl Staenz, Paul Budkewitsch, and Robert A. Neville

Canada Centre for Remote Sensing, National Resources Canada
588 Booth Street, Ottawa, Ontario, Canada K1A 0Y7

Robert Hitchcock
Prologic Systems Ltd.
75 Albert Street, Suite 206, Ottawa, Ontario, Canada K1P 5E7

Christian Nadeau
MacDonald Dettwiler and Associates Ltd.
13800 Commerce Parkway, Richmond, British Columbia, Canada V6V 2J3

ABSTRACT

The study presented in this paper investigated the influence of spatial resolution upon the spectral unmixing for rock/mineral identification and the interpretation for geological mapping in Arctic environments. Probe-1 data acquired near Nanisivik, Nunavut, Canada on July 29, 1999 was used for this purpose. After re-calibrating the cube, its spatial resolution of 6.5 m was degraded using pixel block averaging to generate 13.0-m, 19.5-m, 32.5-m, and 52.0-m data sets. Subsequent processing included the retrieval of surface reflectance using MODTRAN4, automatic endmember selection, and linear spectral unmixing. Ground reference information such as reference spectra of the different target types was used to validate the endmember and unmixing results. The mapping results indicate that the five different rock units examined could be identified successfully across the different spatial resolutions. However, a more detailed delineation of the rock units could be achieved from the data cubes with finer spatial resolution.

1. INTRODUCTION

With the launch of hyperspectral spaceborne sensors, the spatial resolution generally decreases compared to that of airborne systems. Targeting spaceborne systems will provide spatial resolutions in the 20-m to 50-m range for civilian applications[1,2,3]. This will be a challenge for information extraction in many application areas since hyperspectral procedures have been developed and tested on data from airborne sensors with spatial resolutions equal or better than 20 m.

This study concentrates on the effect of spatial resolution on spectral unmixing for mineral mapping purposes in the Canadian Arctic. Probe-1 data with 6.5-m resolution were used to generate data cubes of

spatial resolutions of 13.0 m, 19.5 m, 32.5 m, and 52.0 m. For each cube, the at-sensor radiance was converted to surface reflectance with MODTRAN4. Endmembers were extracted from these surface reflectance cubes by an automated process. Subsequently, these endmembers were used to retrieve rock/mineral-specific abundance maps by a constrained linear spectral unmixing procedure. The resulting endmembers and fraction maps were compared on a qualitative basis. The entire analysis was carried out on the Imaging Spectrometer Data Analysis System (ISDAS)[4], advanced hyperspectral analysis software developed at the Canada Centre for Remote Sensing.

2. TEST SITE

The Borden Rift Basin of northern Baffin Island (N73°/W83°) is characterized by relatively flat-lying Late Proterozoic sedimentary rocks deposited within a deepening rift basin[5]. The area lies within the High Arctic ecozone, characterized by open tundra vegetation and barren rock. Bedrock is abundant and vegetation cover is sparse on the uplands, whereas glacial deposits and mossy grasslands occupy the broad valleys of the lowlands.

The geology of the test site described here consists mainly of dolostones mapped as the Society Cliffs Formation that were later cut by igneous intrusions, presently seen as a series of gabbroic dykes. The dykes are subvertical and orientated along a northwest direction. Bedrock or felsenmeer exposures of the dolostone are generally free of vegetation and lichen cover whereas the surfaced gabbro dykes frequently exhibit a high proportion of encrusting lichen.

3. DATA USED

The hyperspectral data for this study was obtained with the Probe-1 sensor on July 29, 1999 over a test site on Baffin Island, Canada, approximately 30 km west of Nanisivik. The Probe-1 sensor[6] has 128 spectral bands spanning the wavelength range from 437 nm to 2462 nm, with bandwidths between 11 nm and 22 nm. It has a 60-degree field-of-view (FOV), which for the altitude of 2.925 km above ground level corresponds to a swath width of about 3.4 km and 6.5-m pixel size. This sensor is mounted on a three-axis gyro-stabilized platform that compensates for the effects of the aircraft motion for up to 5 degrees for each axis.

Field measurements acquired during the same week as the airborne overflight included the acquisition of ground-based reflectance spectra from geological and vegetated targets using the GER3700™ portable field spectrometer[7]. These measurements also covered a large and relatively uniform outcrop of dolostone, which was used as a calibration target. This instrument was configured with a 10-degree FOV lens, giving a 0.26-m diameter ground FOV from a height of 1.5 m. All measurements were made while the target area was free of any cloud shadows. The target reflectances, derived using a Spectralon™ panel, were then corrected for the panel's reflectance and anisotropy and convolved to the Probe-1 spectral bands. Finally, multiple measurements of a given sample were averaged to yield a mean spectrum for that sample.

4. METHODOLOGICAL APPROACH

4.1 CALIBRATION

The Probe-1 raw data was dark subtracted and trimmed to a width of 512 pixels (across track) to remove the dark current and calibration lamp pixels. Laboratory radiometric coefficients were used to convert the raw data from digital numbers (DN) to radiance.

An initial check of the surface reflectance retrieved from the Probe-1 data and ground-based measurements over the same targets revealed that the laboratory radiometric coefficients were significantly in error throughout the full spectral range of the sensor. Therefore, a reflectance-based vicarious calibration (RBVC) method[6] was used to adjust the Probe-1 radiometric calibration coefficients. This is an iterative numerical technique that adjusts the radiometric coefficients to reduce the absolute difference in every band between the ground-based (calibrating) reflectance spectrum and the reflectance spectrum extracted from the Probe-1 hyperspectral data to within a specified tolerance (0.02 percent absolute in this case). The RBVC method yields a corrected set of radiometric coefficients that convert the hyperspectral data from DN to radiances. These corrected coefficients were applied to the Probe-1 raw data to yield corrected radiance values.

4.2 SPATIAL DEGRADATION

In the next step, the corrected radiance data at the 6.5-m resolution were spatially averaged to yield the desired pixel sizes of 13.0 m, 19.5 m, 32.5 m, and 52.0 m. A mean value was calculated from each of the corresponding pixel blocks, e.g., 2 x 2 window for the 13.0-m resolution. The nature of the pixel degradation process, especially for smaller targets, depends on the starting point of the window. The 6.5-m data were averaged so that the left upper window pixel coincides with pixel 1 and line 1. No attempt was made to compensate for any effects that the spatial averaging might have had upon the signal-to-noise (SNR) of the data. In any case, the SNR of future satellite data is unknown. A detailed discussion on spatial degradation techniques and their application to image data is given in the literature[8,9].

4.3 ATMOSPHERIC CORRECTION

The radiance data were atmospherically corrected prior to the information extraction using a look-up table (LUT) approach[10] with tunable breakpoints to reduce significantly the processing time. The MODTRAN4 code was used in forward mode to generate the radiance LUTs, one for each of a 5% and 60% flat reflectance spectrum. These LUTs were produced for five pixel locations equally spaced across the swath, including nadir and swath edges, for a range of water vapour contents, and for a single aerosol optical depth (horizontal visibility) and a single terrain elevation. The specifications of these parameters and others required for input into the radiative transfer code are listed in Table 1.

Table 1. MODTRAN4 model parameters for the atmospheric correction of the Probe-1 data.

Aircraft heading	179°
Terrain elevation (above sea level)	0.375 km
Sensor altitude (above sea level)	3.300 km
Solar zenith angle	55.6°
Solar azimuth angle	205.6°
Atmospheric model	Subarctic summer
Aerosol model	Continental (rural)
Water vapour content	variable
Ozone column	0.346 cm-atm
CO_2 mixing ratio	357.5 ppm
Horizontal visibility	50 km
Number of streams	8
Wavelength grid interval	4 cm^{-1}

For the retrieval of the surface reflectance, the values in the LUTs were adjusted only for the pixel location in the swath and water vapour content using a bi-linear interpolation routine[11] since single values for the other LUT parameters were used for the entire cube. For this purpose, the water vapour content was estimated for each pixel in the scene with an iterative curve fitting technique[12]. The surface reflectance was then computed for each pixel as described in Staenz and Williams[10]. Figures 1 and 2 show an example of spectra of different target types extracted from the 6.5-m data.

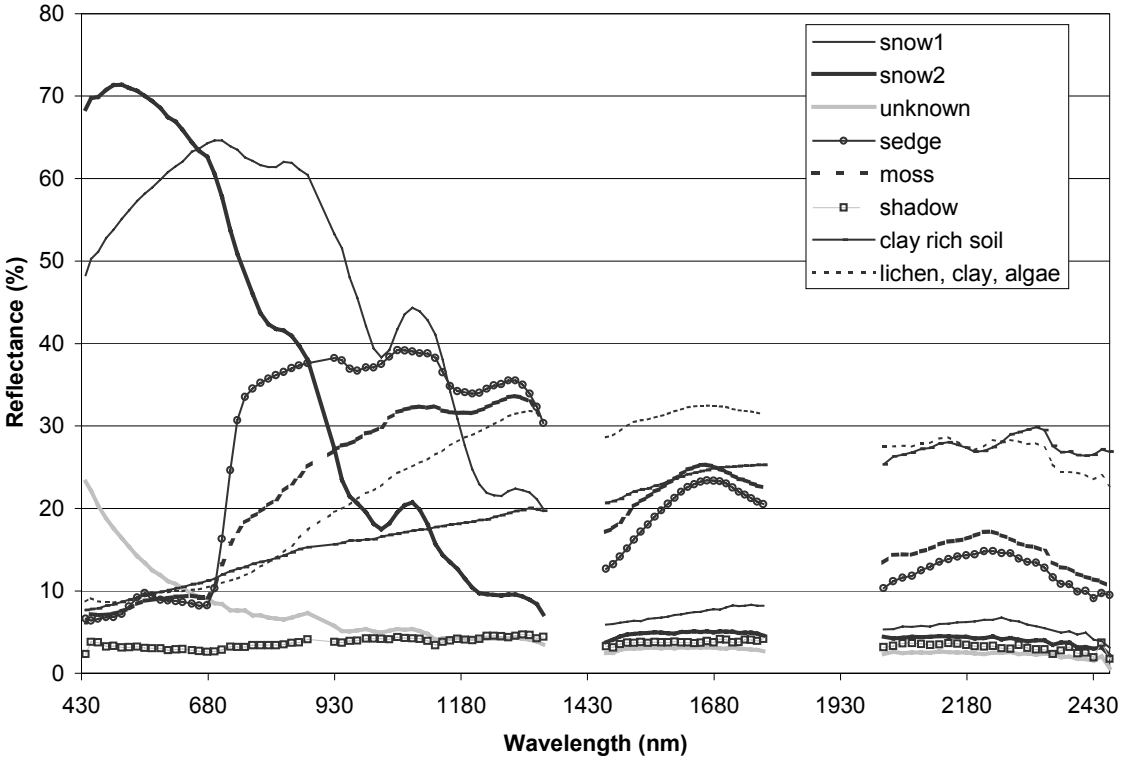

Figure 1: Reflectance spectra of non-rock targets (endmembers).

4.4 ENDMEMBER SELECTION AND SPECTRAL UNMIXING

Endmembers needed for the spectral unmixing were selected from the data cubes themselves using an automated method. The Iterative Error Analysis (IEA)[13] is based on the residual errors generated when a data set is unmixed to find the endmembers. These errors are calculated using a least-square estimate between the previously selected endmember spectrum and the spectrum of each pixel. The errors are also a measure of the distance in N-dimensional space (N = number of bands) between the average spectrum and all the spectra of the data set. To start, the average spectrum of the scene is used to unmix the data set. The next step is to find the pixel or pixels that encompass the largest errors, i.e., that are furthest away from the average spectrum. The user provides the maximum number of pixels forming these endmembers. This first endmember is then used to unmix the image cube, and the average spectrum is discarded. The errors will again be used to find the furthest pixels from the first endmember and will create the second endmember. This process is repeated until the number of endmembers predetermined by the user is reached. Depending on the data sets, up to 30 endmembers have been requested to ensure the extraction of the significant endmembers from the scene.

Once all the endmembers were found, the image cubes were unmixed using a constrained linear technique[14,15], which uses a linear combination of a set of endmember spectra to unmix each pixel

spectrum in the scene into fractions of endmembers constrained to values between o and 1. In addition, the sum of the fractions of a pixel equals 1. The full wavelength range of the Probe-1 sensor was utilised for the endmember selection and spectral unmixing process.

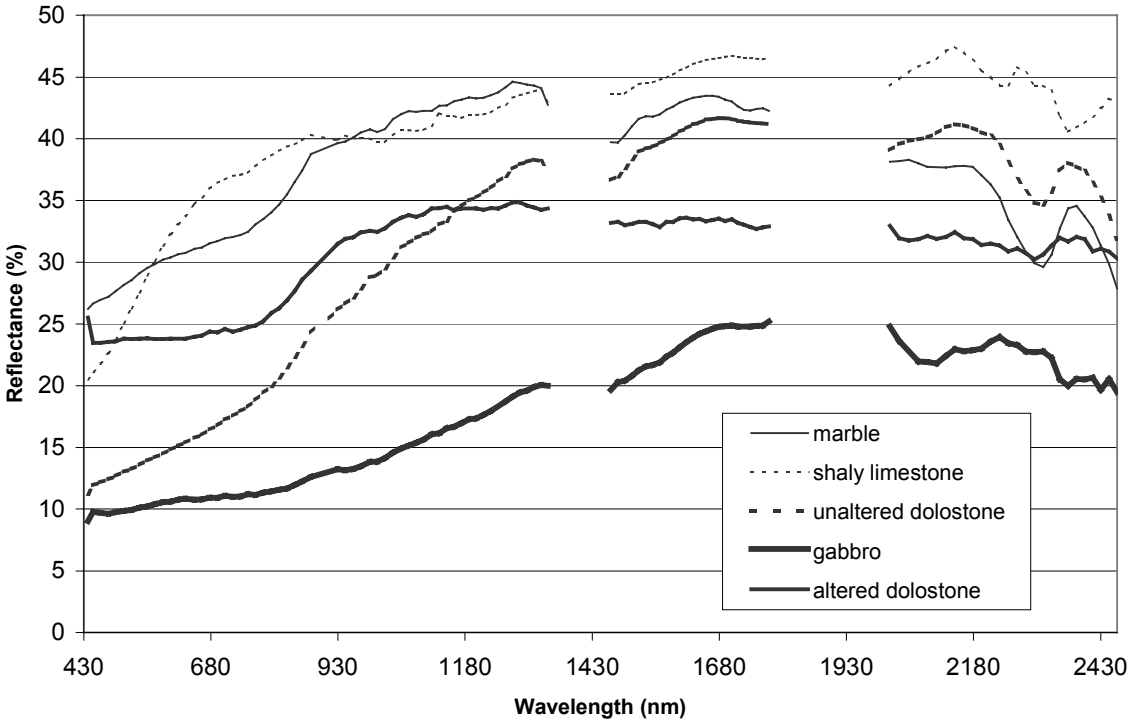

Figure 2: Reflectance spectra of rock targets (endmembers).

5. RESULTS

5.1 ENDMEMBER SELECTION

Tabel 2 lists the endmembers extracted using the automatic IEA technique. These selected endmembers were compared with laboratory and ground-based spectra. Subsequently, they were grouped into 13 single target categories wherever possible. Figures 1 and 2 show reflectance spectra of the different endmember categories retrieved from the 6.5-m data. It can be seen from Table 2 that the same rock endmember types could be extracted from the data cubes after the degradation of the pixel size from 6.5 m to 52.0 m. For example, Figures 3 and 4 show the endmember spectra of marble and gabbro for the different spatial resolutions. The endmembers extracted from the various resolutions differ mainly in amplitude, although the absorption features remain. This is due to the averaging scheme used for this investigation. In general, the spatial extent of the rock outcrop areas is large enough to cover at least one (pure) pixel. This is even the case for the coarser spatial resolutions. Basically the same is valid for the non-rock endmembers with the exception of snow 1. This endmember was not found in the 32.5-m and 52.0-m data. Due to the small patches of snow, it was not possible to pick up a pure pixel for that snow category at these spatial resolutions.

The number of endmembers required to establish the target categories in Table 2 varied from 19 to 29 for the spatially different resolutions. Only 19 endmembers were needed for the 52.0-m resolution data. As previously mentioned, the snow 1 endmember was lost in this case. The required number of endmembers to establish the 13 categories is based on the IEA technique, which selects endmembers in

Table 2: Endmember selected from the spatially averaged image cubes. The numbers in the table indicate the number of endmembers found per target type.

Endmember (Number of Endmembers Required)	**6.5 m** (24)	**13.0 m** (24)	**19.5 m** (29)	**32.5 m** (21)	**52.0 m** (19)
Marble (dolomite)	1	1	1	1	1
Shaly Limestone (calcite, clay)	1	1	1	1	1
Unaltered Dolostone (dolomite)	2	2	2	2	2
Gabbro (lichen covered)	1	1	1	1	1
Altered Dolostone (dolomite)	1	1	1	1	1
Clay-rich Soil	1	1	1	1	1
Mixture of Lichens, Clay, Algae	1	1	1	1	1
Mainly Sedge (heath)	2	1	1	2	1
Mainly Moss (heath)	2	3	3	2	3
Snow 1	2	1	1	0	0
Snow 2	5	4	5	3	3
Unknown	1	1	1	1	1
Shadow	1	1	1	1	1

N-dimensional space, according to the magnitude of the residual errors as described in Section 4.4. The first endmember extracted was generally generated from snow pixels, for all resolutions, because the reflectance of these pixels has the greatest deviation from the mean. Subsequent endmembers alternated between dark pixels, such as shadow, and bright pixels, such as snow and vegetation with the rock endmembers emerging further down the sequence. More snow endmembers were found in the high-resolution data because a greater variety of snow types were resolved. Only one endmember was selected for unmixing when two or more endmembers were extracted for the same target category. In general, the brightest endmember spectrum was selected with exception of the snow categories where an intermediate reflectance spectrum was used for unmixing. Some of the endmembers selected by the IEA technique were not used for subsequent unmixing since they represent a mixing of two endmembers identified as rock/mineral units

5.2 SPECTRAL UNMIXING

The 13 endmembers representing the target categories in Table 2 were used to unmix the spatially different data cubes up to 19.5 m on a pixel basis. Only 12 endmembers were included for the 32.5-m and 52.0-m data cubes since the snow 1 endmember could not be retrieved. An examination of each error image, derived from unmixing the different data sets, revealed an average residual error of up to 1.5 % and, hence, one can be confident all major endmembers have been found. The unmixing results indicate that the main rock types (unaltered and altered dolostone, gabbro, marble, limestone) show up in the different fraction images regardless of the spatial resolution considered for this investigation. Figure 3 shows fraction images of the gabbro rock unit across the different spatial resolutions. The fraction of each pixel is indicated by a grey tone with black representing a low abundance value, white a high value. These images show that some detail is lost with increasingly coarser resolutions. Despite this fact, the basic rock type is clearly identified. This is generally also true for all the other rock endmembers, including a minor rock unit of marble, that could be detected even in the 32.5-m and 52.0-m data (Figure 4). The marble, in contact with the gabbro dyke, is indicated by the bright grey-tone pixels (high abunadances) and is mainly located in the lower right part of the imagery. Most of the thinner exposure of marble located towards the centre and upper left of the fraction image were lost at the 52.0-m spatial resolution.

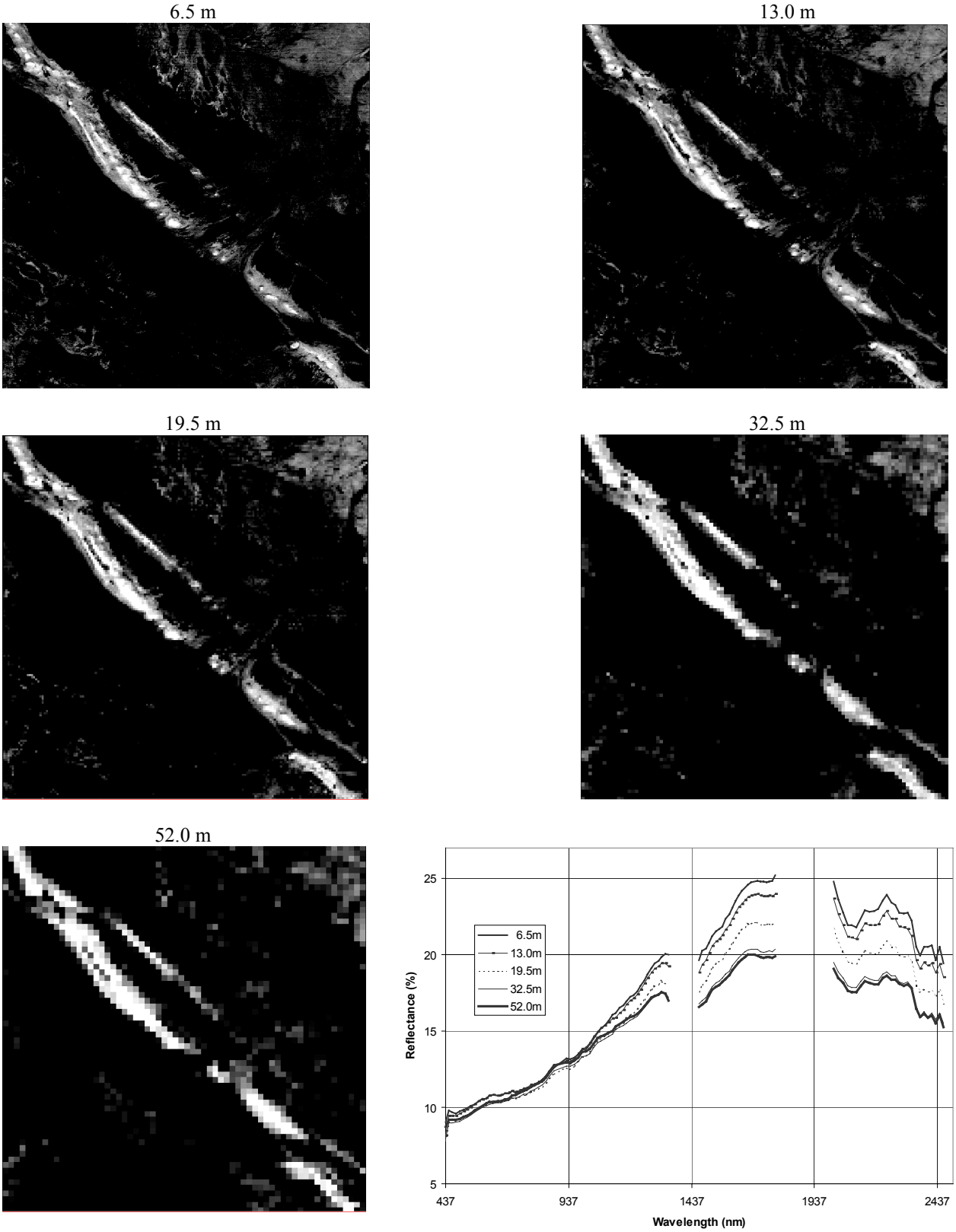

Figure 3: Image fractions maps for the occurrence of gabbro at different spatial resolutions and associated endmember spectra (bottom right).

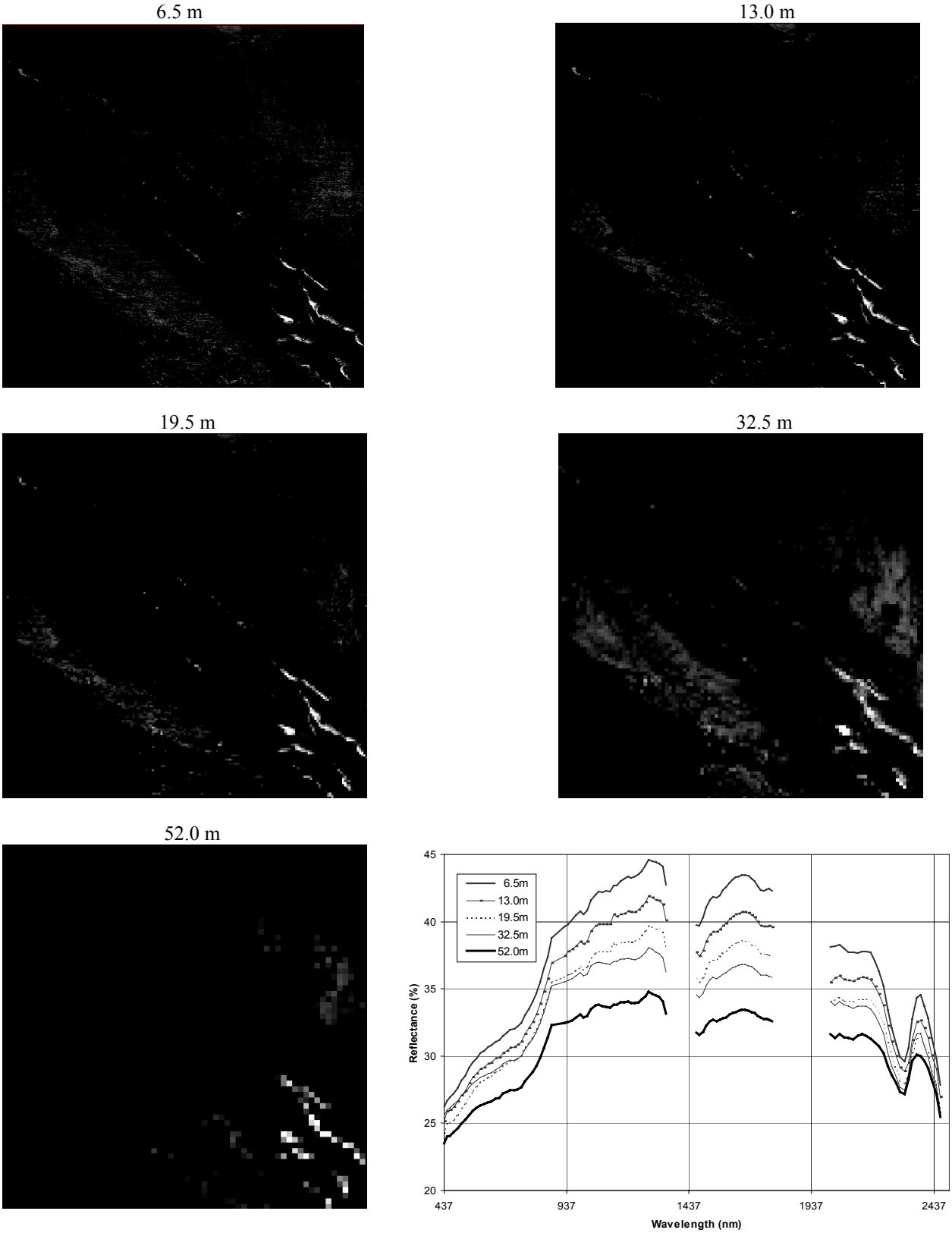

Figure 4: Image fractions maps of marble (dolomite) at different spatial resolutions and associated endmember spectra (bottom right).

6. CONCLUSIONS

The objective of this study was to investigate the impact of spatial resolution upon the identification and mapping of rock/mineral units for future satellite data acquisition in Arctic environments. Probe-1 radiance data was degraded from 6.5-m to 13.0 m, 19.5 m, 32.5 m, and 52.0 m after re-calibration of the data cube. Subsequent data pre-processing included atmospheric correction using MODTRAN4. The resulting surface reflectance data were processed using the automatic IEA technique to extract the endmembers. The endmembers extracted were categorized into 13 target types with exception of the 32.5-m and 52.0-m resolution data where one of the two snow categories was lost. Both the reflectance data and associated endmembers were used to generate the fraction maps via constrained linear spectral unmixing for each spatial resolution. The results indicate that the areal coverage of the rock units were mapped similarly across the different spatial resolutions although detailed information was lost for the coarser spatial resolutions. These results are encouraging for the identification and geological mapping of rock/mineral units with resolutions in the 30-m to 50-m range. Such a resolution is available from the existing spaceborne sensor Hyperion[1] as well as proposed for future sensors such as the Compact High Resolution Imager (CHRIS)[2] and the Naval Earth Map Observer (NEMO)[16].

7. ACKNOWLEDGEMENTS

The authors wish to thank John Gingerich (Noranda Mining and Exploration Inc.) for facilitating logistics for the Probe-1 data collection campaign over Baffin Island. Logistical support from the Polar Continental Shelf Project (contribution #014-01) for field validation is gratefully acknowledged. We thank Ron Sutherland and Don Sangster for stimulating discussions on the geology of the area. CCRS acknowledges the financial support for this project by Barrick Gold Corp., Cameco, Cominco Ltd., De Beers Consolidated Mines Ltd., Falconbridge Limited, Noranda Mining and Exploration Inc., and Placer Dome Exploration Inc. The authors wish to thank the Hamlet of Arctic Bay and Arqvartuuq Services Ltd. for their co-operation and the assistance of Larry Oyukuluk in the field. The courtesy of the staff at the Nanisivik Mine and access to facilities during the summer of 2000 is sincerely appreciated.

8. REFERENCES

1) Folkman, M., J. Pearlman, L. Liao, P. Jarecke, 2000, "EO-1/Hyperion Hyperspectral Imager Design, Development, Characterization, and Calibration", *Proceedings of the International SPIE Conference on Hyperspectral Remote Sensing of the Land and Atmosphere*, Sendai, Japan, Vol. 4151, pp. 40-51.

2) ESA, 2000, "Announcement of Opportunity: Exploitation of CHRIS Data from the PROBA Mission", *ESA Scientific Campaign Unit*, ESTEC, Nordwijk, The Netherlands, No. 64, pp. 10-12.

3) Perkinson, M.-C., D. Lobb, M. Cutter, and R. Renton, 2001, "Low Cost Hyperspectral Imaging from Space", *Proceedings of the 3rd International Symposium on Small Satellites for Earth Observation*, Berlin, Germany, pp. 199-202.

4) Staenz, K., T. Szeredi, and J. Schwarz, 1998, "ISDAS - A System for Processing/Analyzing Hyperspectral Data", *Canadian Journal of Remote Sensing*, 24(2): 99-113.

5) Jackson, G.D. and Sangster, D.F., 1987, "Geology and Resource Potential of a Proposed National Park, Bylot Island and Northwest Baffin Island, Northwest Territories, *Geological Survey of Canada*, Ottawa, Paper 87-17, 31pages.

6) Secker, J., K. Staenz, R.P. Gauthier, and B. Budkewitsch, 2000, "Vicarious Calibration of Hyperspectral Sensors in Operational Environments", *Remote Sensing of Environment*, 76: 81-92.

7) GER 3700, 1997, "GER 3700 Spectroradiometer", *User Manual Version 2.0*, Geophysical & Environmental Research Corp., Millbrook, New York, U.S.A., 59 pages.

8) Justice, C.O., B.L. Markham, J.R.G. Townshend, R.L. Kennard, 1989, "Spatial Degradation of Satellite Data", *International Journal of Remote Sensing*, 10(9): 1539-1561.

9) Townshend, J.R.G., C.O. Justice, W. Li, C. Gurney, and J. McManus, 1991, "Global Land Cover Classification by Remote Sensing: Present Capabilities and Future Possibilities*", Remote Sensing of Environment*, 35: 243-255.

10) Staenz, K., and D.J. Williams, 1997, "Retrieval of Surface Reflectance from Hyperspectral Data Using a Look-Up Table Approach", *Canadian Journal of Remote Sensing*, 23(4): 354-368.

11) Press, W.H., S.A. Teukolsky, W.T. Vetterling, and B.P. Flannery, 1992, "Numerical Recipes in C", *Cambridge University Press*, Cambridge, England, pp. 123-125.

12) Staenz, K., T. Szeredi, R.J. Brown, H. McNairn, and R. VanAcker, 1997, "Hyperspectral Information Extraction Techniques Applied to Agricultural *casi* Data for Detection of Within-Field Variations", *Proceedings of the International Symposium in the Era of Radarsat and the Nineteenth Canadian Symposium on Remote Sensing*, Ottawa, Ontario, Canada, 8 pages (CD-ROM).

13) Szeredi, T., Staenz, K., and Neville, R.A., 2001, "Automatic Endmember Selection : Part I Theory", *Remote Sensing of Environment* (submitted).

14) Shimabukuru, Y.E., and Smith, J.A., 1991, "The Least Squares Mixing Models to Generate Fraction Images Derived From Remote Sensing on Multispectral Data*", IEEE Transactions on Geoscience and Remote Sensing*, 29: 16-20.

15) Boardman, J.W., 1995, "Analysis, Understanding and Visualization of Hyperspectral Data as Convex Sets in n-Space", *Proceedings of the International SPIE Symposium on Imaging Spectrometry*, Orlando, Florida, U.S.A., Vol. 2480, pp. 23-36.

16) Wilson, T., and C. Davis, 2000, "Naval EarthMap Observer (NEMO) Satellite", *Proceedings of the International SPIE on Imaging Spectrometry V*, Boulder, Colorado, U.S.A., Vol. 3753, pp. 2-11.